



Evaluation of Continuous Epoxy-Impregnated Carbon Fibre Reinforcement in a 3D-Printable Geopolymer Composite

Mona Sando¹ , Sara Alves Santos² , Paul Worms² , Aleksander Gurlo² ,
and Dietmar Stephan^{1,*} 

¹Building Materials and Construction Chemistry, TU Berlin, Gustav-Meyer-Allee 25, 13355 Berlin, Germany

²Advanced Ceramic Materials, TU Berlin, Hardenbergstraße 40, 10623 Berlin, Germany

*Correspondence: Dietmar Stephan, stephan@tu-berlin.de

Abstract. This study investigates the potential of geopolymer reinforcement for extrusion-based 3D printing using in-situ impregnation of continuous carbon fibre. The geopolymer is composed of fly ash, ground granulated blast furnace slag and an activator, specifically developed for 3D printing. Although 3DCP has seen significant advancements in recent years, structural reinforcement remains a largely unresolved challenge. In conventional concrete construction, steel reinforcement is used to withstand tensile forces that cannot be absorbed by the mineral building material alone, creating the composite material reinforced concrete. For additive manufacturing to remain competitive, printed concrete must offer comparable quality and performance, without compromising the benefits of geometric freedom, digital design, and automation. The use of continuous carbon fibre strands with a functional epoxy resin infiltration enables strong adhesion between the fibre and the geopolymer matrix, allowing for layer-wise reinforcement in tensile zones. Moreover, clinker-free geopolymers activated by highly alkaline solutions offer a more sustainable alternative by significantly reducing CO₂ emissions. Various combinations of geopolymer matrix and carbon fibre reinforcement are evaluated through three-point bending tests to determine flexural tensile strength, and through pull-out tests to assess peak load. Microscopic investigations using light microscopy and scanning electron microscopy (SEM) are conducted to analyse the interfacial bonding between fibre, geopolymer, and epoxy resin. The results demonstrate that embedding impregnated fibres "fresh-in-fresh" provides the most effective fibre–mortar bond, without limiting shape flexibility during printing.

Keywords: Geopolymer, Continuous Fibre Reinforcement, Carbon Fibre Impregnation, Fresh-in-Fresh-Embedding, Pullout Strength, Flexural Strength, Fibre-Matrix Adhesion, Microstructural Analysis

1. Introduction and Motivation

3D concrete printing (3DCP) is fundamentally transforming the construction sector, offering significant advantages like greater geometric freedom, enhanced digital design, and increased automation. This is achieved by building structures layer by layer [1]. Using clinker-free geopolymers, activated by highly alkaline solutions, provides a more sustainable choice by considerably limiting CO₂ emissions. This aligns well with ongoing efforts towards environmentally friendlier building methods [2,3].

Despite these advances, the inherent anisotropic behaviour and generally lower tensile strength of 3D printed concrete structures are key limitations. In traditional building, steel reinforcement is fundamental for resisting tensile forces and ensuring structural integrity. For 3DCP to gain widespread acceptance and stay competitive, reinforcement strategies must be both effective and compatible with the high degree of design freedom. Integrating traditional, rigid steel reinforcement into the automated, layer-by-layer 3D printing process presents considerable difficulties. This highlights a critical need for novel, adaptable reinforcement solutions that can be integrated into the printing process, providing the necessary tensile capacity without compromising the benefits of digital fabrication [4,5].

Compared with conventional steel reinforcement, carbon fibre strands offer a much higher strength-to-weight ratio; they are up to four times lighter and up to six times stronger [6]. They are also flexible in placement, which facilitates construction, and the reduced need for concrete cover lowers material use. Continuous fibres outperform discontinuous ones by providing uninterrupted stress paths, more efficient load transfer, higher directional stiffness and strength, and the ability to bridge wider cracks, whereas short fibres transfer stresses in multiple directions but lose efficiency at their ends [7,8]. In practice, continuous systems can simplify handling during transport and placement compared with long steel bars, although processing may require specialised cutting or winding equipment. These properties make continuous carbon fibres particularly suitable for advanced cementitious or geopolymer systems. An example of continuous carbon fibre reinforcement is the Stress-Ribbon Footbridge built at TU Berlin; a design approach based on active vibration control in which the open-jointed concrete plates are supported by CFRP ribbons [9]. However, carbon fibres are still expensive, with continuous fibres being particularly costly compared with steel or discontinuous fibre alternatives, fail in a brittle rather than ductile manner, and have lower fire resistance [9–12].

This study investigates the effectiveness of epoxy-impregnated continuous carbon fibre strands as reinforcement for extrusion-based 3D printing. A print head, currently under development at TU Berlin, enables the integration of these fibres directly into the printing path. The system includes a fibre impregnation unit, a cutting device, and a fibre placement mechanism, enabling the embedding of freshly impregnated continuous carbon fibre strands during printing. The focus of this study lies on evaluating the reinforcement performance of this method. A specially designed geopolymer mixture, composed of fly ash (FA), ground granulated blast furnace slag (GGBFS) and an activator, serves as the matrix material. The research investigates how the strong bond provided by the epoxy (EP) infiltration supports effective reinforcement in tensile zones between printed layers. To assess the mechanical performance, different carbon embedding methods are tested using three-point bending tests to determine flexural tensile strength, and pullout tests to evaluate the fibre–matrix bond. Additional insights into the fibre–geopolymer–resin interface are gained through the use of light microscopy and scanning electron microscopy (SEM).

2. State of the Art

In 3DCP, various reinforcement methods have been developed, each with its own advantages and limitations [13,14]. Post-installed reinforcement uses traditional steel bars placed after printing, often by filling a printed shell with concrete. It provides strong support but requires a significant amount of manual work, which limits automation [15]. Pre-installed reinforcement places the bars before printing, with concrete printed around them. It is useful for vertical elements such as walls, but it only works for simple shapes and also requires manual effort [16]. The most common approach involves incorporating short fibres (e.g., basalt, glass, steel, polymers, carbon, typically 3–8 mm) into the mix before printing. These fibres can carry tension and can bridge small cracks after hardening. While easy to mix in, a high fibre content can impede extrusion through small nozzles, often reducing workability and negatively influencing interlayer bonding and its surface finish [17,18].

Mesh reinforcement is an approach where mesh is printed together with the concrete using a special nozzle. The mesh is overlapped layer by layer, giving strength in both horizontal and vertical directions [14]. Continuous fibre integration uses long fibres placed along the printed path, offering strong and continuous support. Earlier methods often placed fibre strands or ropes manually between layers. Some researchers have used robotic arms or special nozzles to add continuous fibres during printing. These methods aim to provide high directional strength using materials such as carbon or glass fibres [8,19]. Lim et al. [20] used continuous twisted stainless-steel wires with short polymer fibre hybridisation to improve bond and bridge microcracks. However, this method can limit the creation of complex, free-form geometries due to the low flexibility of the wire.

Demont et al. [21] developed a Flow-Based Pultrusion (FBP) methodology for 3DCP with in-situ reinforcement, which is a motorless technology that relies on the flow of mortar extrusion to pull continuous glass or basalt fibre. The main limiting factor of this approach is the yield stress of the fibre relative to the pull-out force. This technology has the potential to unlock complex design constraints in traditional manufacturing, enabling the production of strong, lightweight structures. Mineral-impregnated continuous carbon fibres (MCFs) provide a corrosion-resistant and chemically stable alternative to steel and polymer reinforcements, making them well-suited for use in aggressive environments and advanced construction methods such as 3DCP [8,22,23]. Surface sizing improves the wettability of the fibres by reducing the contact angle with cementitious matrices, which enhances infiltration, minimises porosity, and strengthens the fibre–matrix bond [23,24]. The mineral impregnation has a significant impact on adhesion and mechanical performance [23]. Beyond bonding, mineral impregnation protects the brittle fibres from surface damage and abrasion, thus increasing their durability. Continuous fibres support efficient load transfer and controlled crack formation, contributing to improved long-term behaviour of reinforced cementitious materials. Depending on the application, impregnated fibres can be integrated into 3D printed mortars in either a fresh, flexible state or after hardening, offering design adaptability and structural efficiency [8].

To improve shear force transfer, carbon fibres were impregnated with an EP resin to enhance adhesion to the concrete matrix and boost the performance of concrete slabs. This application focuses on conventional manufacturing processes rather than 3D printing [25]. Recent studies highlight innovative coating and delayed-curing approaches to improve the bond strength and flexibility of carbon-fibre reinforcement in concrete. Coating methods can increase tensile strength and durability, but often reduce formability [26]. In contrast, carbon fibres impregnated with resin and cured after placement allow highly shapeable reinforcement for extrusion and 3D-printing applications. However, curing inside fresh concrete is influenced by its humid, alkaline environment and demands careful timing and reliable in-process heating, which still limits large-scale use in additive manufacturing [27–29].

A key parameter for assessing fibre–matrix interaction efficiency is the pullout resistance, often expressed as interfacial bond strength (IBS) [30–32]. This reflects the mechanical interlock and adhesive bonding between reinforcement and matrix. According to Eurocode 2 [31], the bond strength in conventional reinforced concrete is influenced by factors such as compressive strength, surface texture of the reinforcement, cross-section, concrete cover depth, transverse reinforcement, and anchorage length. Ribbed bars generally show higher bond strength due to improved mechanical interlock.

For stranded steel fibres in cementitious matrices, Yuan et al. [32] reported IBS values ranging from 6 to 13 MPa, depending on fibre diameter, w/c ratio, and embedment length. Bilek et al. [30] observed that increased binder content leads to higher IBS and indicated bond strengths for Portland cement-based and alkali-activated concrete reinforced with smooth steel bars ranging from 2.5 to 5 MPa. Alberti et al. [33] found bond strengths around 5 MPa for polyolefin macro-fibres in self-compacting concrete. For concrete with glass-fibre-reinforced polymer bars, pullout tests indicated that surface morphology is critical, with sand-coated or ribbed bars reaching average values of nearly 12 MPa [34].

According to [35], in 3D concrete printing, the bond strength of post-installed reinforcement depends on the printing direction. Ribbed bars exhibited IBS values ranging from 19 to 30 MPa, while smooth wires reached only 0.6 to 4.3 MPa [35]. Duan et al. [36] further investigated the influence of printing speed on the bond behaviour of continuous glass fibres. Neef et al. [8] highlighted that the manufacturing method - whether extruded, cast, or printed - also affects bond strength, complicating direct comparisons. Given the wide range of influencing factors, consistent benchmarking of IBS remains challenging.

Despite these varied approaches, a significant gap remains in achieving truly robust, automated, flexible, and inline reinforcement solutions for 3D printed structures. Current methods often compromise automation, geometric freedom, or reliable bond performance. Specifically, the challenges of achieving strong, flexible, and corrosion-resistant continuous reinforcement that seamlessly integrates with the printing process remain to be addressed. The reinforcement proposed in this study, a highly flexible, EP-impregnated, ribbed carbon fibre roving, aims to address these limitations by enhancing the fibre-matrix bond, preventing pullout, and eliminating the need for external fibre treatment, all without negatively affecting the workability or interlayer bonding of the mortar.

3. Fibre Integration

Continuous fibres, widely used in advanced composites such as Carbon Fibre Reinforced Polymers (CFRPs), have attracted growing interest as reinforcement due to their strength-to-weight ratio, low density, fatigue resistance, and potential for 3D printing integration, enabling design flexibility [37]. Continuous carbon fibre can exhibit a tensile strength one order of magnitude greater than steel while holding low density [38].

Fibres like basalt, glass, and carbon can be used to reinforce concrete. While basalt fibres offer good tensile strength and a greener footprint, they are susceptible to alkali attack [39]. General-purpose glass fibres are cheaper but very sensitive to alkali environments; alkali-resistant versions address this issue, but at the expense of lower stiffness and creep resistance [40]. Carbon fibre, though more expensive, offers very high tensile strength, stiffness, creep resistance, and excellent alkali resistance, making it ideal for high-performance structural uses [41]. Both short and continuous fibres can be used, with the latter offering superior performance due to its continuity, leading to higher overall strength and stiffness [42].

Continuous fibres are prone to mechanical issues like slippage or displacement when cracks form, and bridging (fibre strands entangling due to matrix delamination) [43,44]. Choosing an appropriate matrix is vital to enhance the fibre-concrete bond and ensure good load transfer. Thermosets, such as EP resins, establish strong covalent cross-links when cured, becoming hard and rigid, and generally exhibit higher resistance to chemical corrosion than thermoplastics or even metals [45,46]. In fresh mortar, uncured resin adheres to the paste by mechanical and chemical interlocking – fluid resin moulds to nearby capillary pores and micro-roughness in the mortar, becoming anchored as the concrete cures, with the resin adhering to the surface via van der Waals forces [47].

The investigation into EP-based continuous carbon fibre reinforcement for geopolymer applications has not been well explored. It is unknown whether the use of uncured fibre in geopolymer mortar could have the desired effect. This research aims to investigate the application of uncured EP-based continuous carbon fibre reinforcement in a geopolymer, offering a new perspective for the future of additive manufacturing with geopolymers.

4. Materials and Methods

4.1 Geopolymer Formulation and Sample Preparation

The geopolymer was prepared under laboratory conditions (65% relative humidity, 20 °C), based on 1 kg of solids, using 611 g fly ash (FA), 68 g fine FA, 94 g ground granulated blast furnace slag (GGBFS), 226 g quartz sand, and the liquid components: 126 g water, 129 g sodium hydroxide (50 wt%), and 18 g sodium silicate. The fresh geopolymer exhibited a density of 2.04 kg/L. Mixing followed the procedure specified in EN 196-1 [48], with sodium hydroxide and water premixed and added simultaneously with sodium silicate to the dry components. The total mixing time was 6 min [2,3,49]. The oxide composition and further material properties are provided in a previous study [2,3].

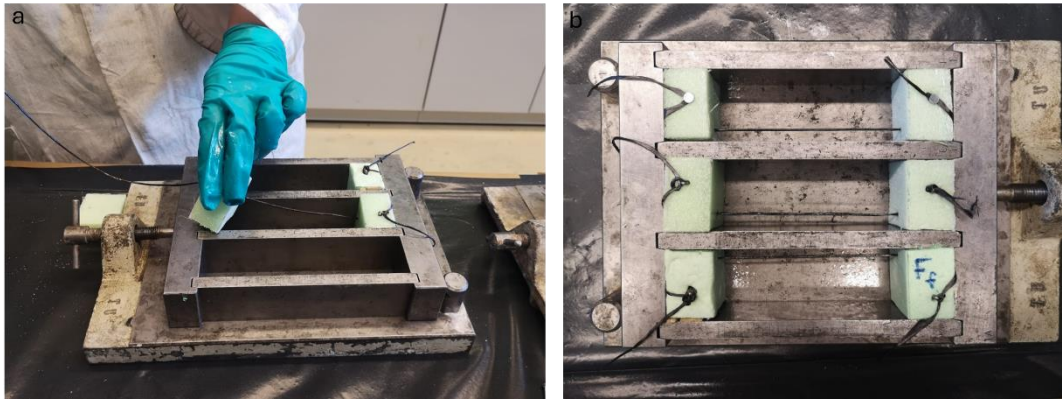


Figure 1. Sample preparation for 3-point-bending test with (a) fibre integration guided through extruded polystyrene blocks and (b) prepared prism mould with fibre placement in the centre of bottom side with a mortar cover of 5 mm.

For the three-point bending test, prismatic specimens with dimensions of 110·40·40 mm³ were prepared using a standard mould according to EN 196-1 [48]. Figure 1 visualises the integration of the fibre centrally on the bottom side of the mould, with a mortar cover of 5 mm, using precisely fitting extruded polystyrene (XPS) blocks with the dimensions of 25·40·40 mm³ and a small cut-out for fibre placement. The flexible fibre was guided through the blocks and fixed in place using a pin (see Figure 1a). The mortar was cast into the mould using a vibrating table, with clamping the mould onto it. The XPS blocks were secured with an additional plate to prevent displacement due to mechanical vibration. After preparation, the moulds were covered with foil and stored at laboratory conditions. After demoulding within a sample age of 24h, the specimens were stored in locked boxes at 100% relative humidity and 20°C until testing.

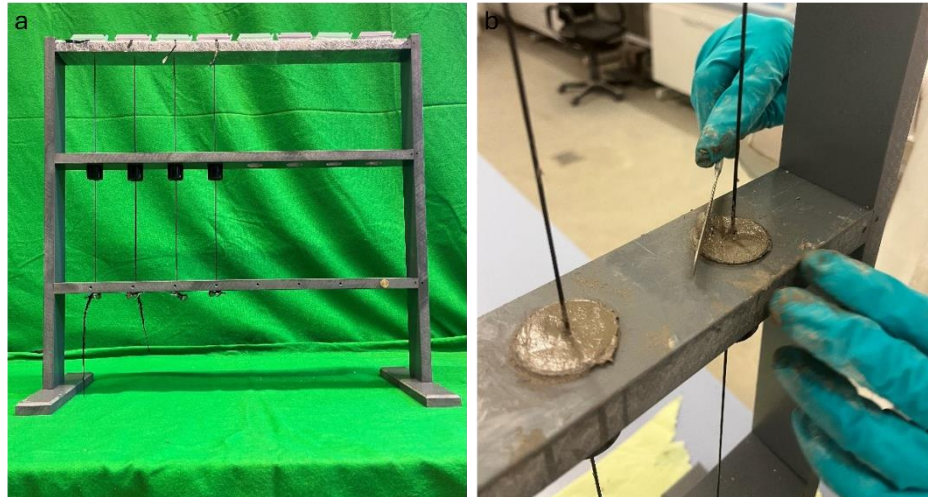


Figure 2. Sample preparation using a (a) custom-made sample holder and (b) mould filling with a spatula.

For the pullout tests, the samples were prepared using a custom-made sample holder (Figure 2a). The moulds, which were fixed into the middle beam of the sample holder, had a cylindrical shape with a diameter of 30 mm and a height of 48 mm. Each mould had a closed base with a central opening of 2 mm for fibre insertion. The fibre was passed through aligned openings in the vertical and was accurately fixed at both the top and bottom beams of the sample holder. The mortar was poured into the moulds manually using a spatula (Figure 2b). Care was taken to ensure that the fibre remained free of mortar outside the mould. After preparation, the samples were covered with foil and stored under laboratory conditions until testing.

4.2 Resin Impregnation

A novel impregnation system was developed (Figure 3), consisting of a 50 cc syringe barrel (Vieweg GmbH, Kranzberg, Germany) and fully adaptable 3D-printed components designed at TU Berlin. These included a meander unit, a nozzle (with 0°, 45° and 90° angles), a top cap, and a syringe holder (Figure 3b). All components were printed using stereolithography (SLA) and provided sufficient transparency to allow visual monitoring of the impregnation process. This enabled clear identification of parameters such as resin flow with the use of coloured dye in transparent resin and formation of air voids. The central element of the system was the meander unit (Figure 3a), which served as both fibre guide and impregnation element. It incorporated two mirrored plates with opposing curved surfaces; a 0.5 mm overlap ensured a slight compression of the fibre bundle while reducing friction. The curvature points generated pressure zones that promoted fibre spreading and resin impregnation. Both plates were magnetically fixed in each corner, allowing for precise alignment and easy disassembly for cleaning. The meander design, including number of windings, plate spacing and length, was optimised to minimise the fibre extraction force and reduce air bubble formation in the resin. The top cap acted as a protective barrier against the external environment while also aligning and flattening the fibre.

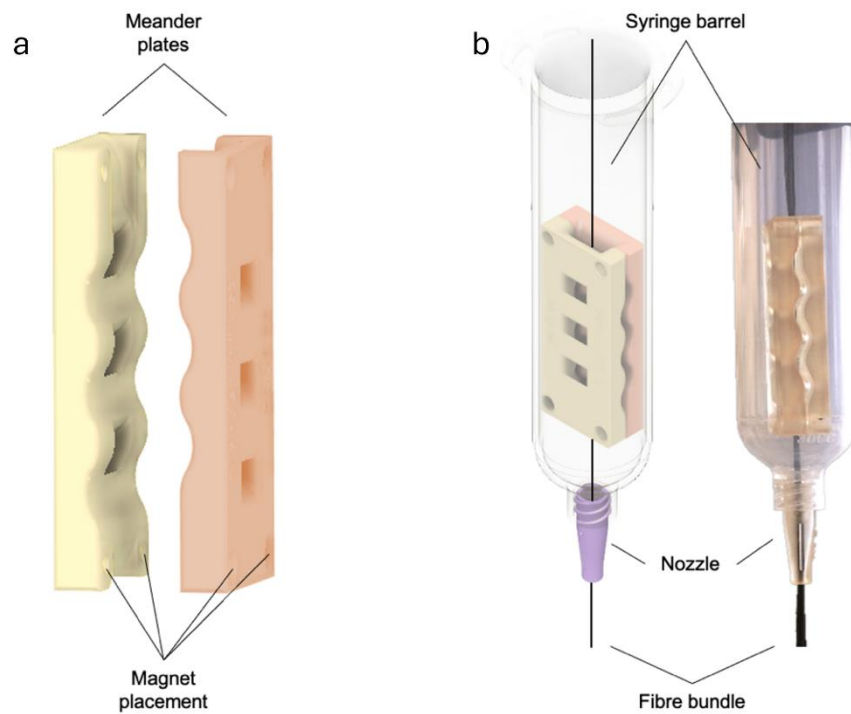


Figure 3. Visualisation of the fibre impregnation system; (a) CAD design of meander consisting of two mirrored structures with matching hills and valleys, and (b) CAD design with 0° angle nozzle (left) and 3D printed prototype (right) of impregnation setup with continuous fibre placement.

For the laboratory tests, the fibres were impregnated using the test stand shown in Figure 4. The setup included the impregnation unit with a syringe holder as the attachment point for the entire impregnation system and, acting as an interface for future 3D-printing applications, a fibre spool mounted on ball bearings to reduce friction and a drawing unit equipped with a motorised wheel. The impregnated fibres could be drawn at speeds of 10 cm/s and 20 cm/s. An Arduino board controlled a stepper motor that adjusted the extraction speed. When the motor operated, a force sensor measured the resistance exerted by the fibre, acting in the opposite direction to gravity. This measured force was then used to calculate the tensile resistance of the fibre during the impregnation process. For 3D printing, a fibre impregnation unit is integrated into the printhead (see Figure 13).

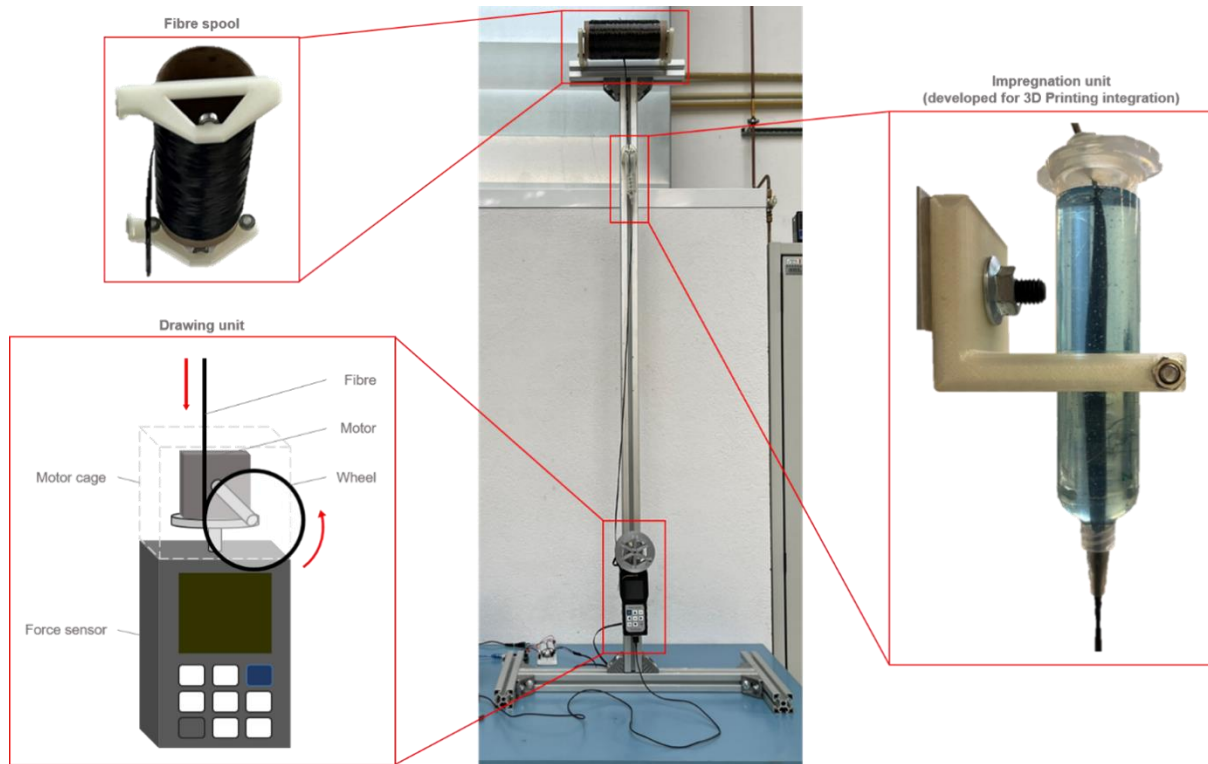


Figure 4. Test stand featuring the developed impregnation system for producing CFRP specimens.

For the experimental investigations in this study, continuous carbon fibres of a standard industrial type (24k, 830 tex) from Teijin Carbon Europe GmbH (Wuppertal, Germany) were impregnated with Resin 1 (Table 1), using a 0° angle nozzle and were manually drawn with an approx. speed of 10 cm/s to produce carbon fibre reinforced polymer (CFRP) specimens. The fibres were either placed freshly impregnated into the geopolymer matrix or first cured horizontally at room temperature for 24h after impregnation, and then introduced into the matrix (see Section 4.1). The mass of resin in the impregnated fibre strand at a speed of 10 cm/s was measured to be approx. 0.010 g/cm. Using the epoxy resin density of 1.2 g/cm³, this corresponds to a resin volume of approx. 0.0090 cm³/cm.

4.2.1 Screening Tests

Screening tests were conducted to select the optimal resin for fibre impregnation. For these tests, continuous carbon fibres, 12k (800 tex, E-modulus 244 kN/mm²) and 24k (830 tex, E-modulus 286 kN/mm²), from Teijin Carbon Europe GmbH (Wuppertal, Germany) were impregnated with two different thermoset resin systems. The key processing parameters and material properties for Resin 1 (R1) and Resin 2 (R2) are summarised in Table 1.

To assess tensile performance, the CFRP specimens were extracted at speeds of 10 cm/s and 20 cm/s using a test stand (Figure 4). After impregnation, each fibre was cut to a length of 1m, horizontally suspended during a 3-day curing period at room temperature (RT), and then segmented into sub-samples of 250 ± 5 mm. Specially developed sample holders (see Figure 6a), designed at TU Berlin, were securely clamped to both ends of each specimen for tensile testing.

The results of the force measurements for fibre extraction at both extraction speeds (Table 1) show an increase in tensile force with higher drawing velocity for both resin systems, with the effect being more pronounced in the case of R1. As also indicated in Table 1, the viscosities of the base resins and hardeners, combined with their respective mixing ratios, result in comparable overall mixture viscosities. According to the viscosity blending rule, this suggests that the observed differences in extraction resistance lies in the mechanical interlocking between

fibre and resin. The R1 system may counteract sudden displacement more effectively, suggesting stronger interfacial bonding.

Table 1. Overview of processing parameters, material properties of thermoset resin systems, and corresponding fibre extraction forces at different drawing speeds.

Parameter	Resin 1	Resin 2
Processing time	approx. 50 min	approx. 90 min
Curing time (RT*)	24h	16-24h
Mixing ratio (base:hardener)	100:40	100:25
Viscosity _{base}	750 ± 150 mPas	700 ± 70 mPas
Viscosity _{hardener}	75 ± 25 mPas	< 40 mPas
Extraction force (12k, 10 cm/s)	3.83 N	1.62 N
Extraction force (12k, 20 cm/s)	4.63 N	1.77 N
Extraction force (24k, 10 cm/s)	3.58 N	3.44 N
Extraction force (24k, 20 cm/s)	4.41 N	3.93 N

* RT: room temperature

To evaluate the mechanical properties of the CFRP and to better understand whether adhesion mechanisms contribute to the observed friction differences during extraction, tensile tests were conducted for both fibre types (12k and 24k) with R1 and R2 at extraction speeds of 10 cm/s and 20 cm/s.

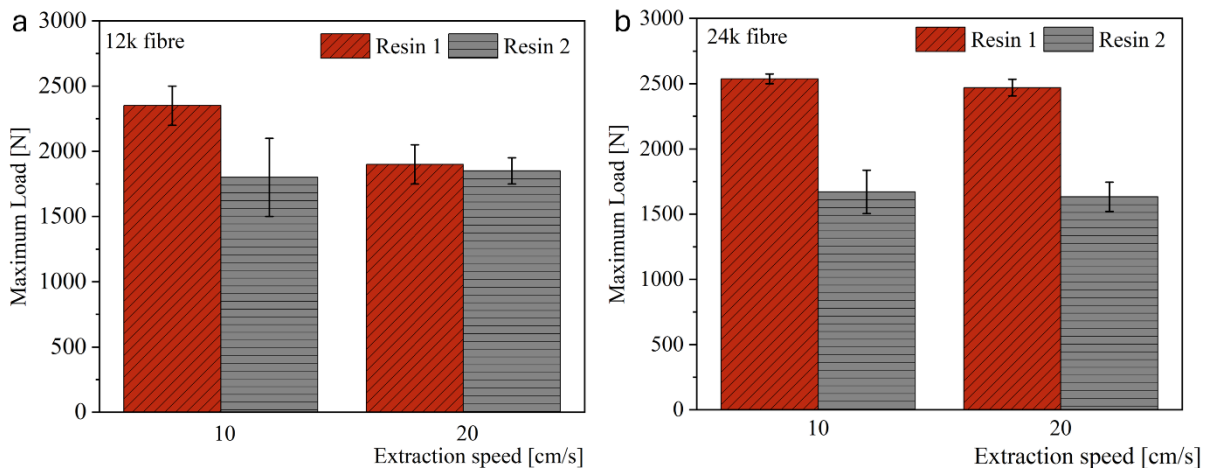


Figure 5. Results of CFRP tensile tests produced at different extraction speeds for (a) 12k fibres and (b) 24k fibres.

Figure 5 shows that at an extraction speed of 10 cm/s, CFRP with R1 exhibited higher load at break for both fibre types compared to those with R2. This supports the tensile force results (Table 1) and suggests that the observed resistance is likely linked to the strength of the fibre-resin interfacial adhesion. As the extraction speed increases, the impregnation time also decreases, affecting the bonding strength at the fibre-resin interface. Given a constant impregnation length, the impregnation time is greater at lower extraction speeds (10 cm/s), allowing the resin more time to infiltrate the fibre bundle and adhere to the fibre surface, which may increase the strength of the fibre-resin interface. In this case, composites drawn at lower speeds may have a higher resin content, although it does not exceed the maximum allowable amount determined by the nozzle diameter. It is also possible that, at higher extraction speeds, the fibre movement drags more air into the resin, which remains trapped and creates pores in the matrix – weak points that enable crack propagation and affect the strength of the composite material. The extraction speeds used in this work are well aligned with the printing speeds achievable by the robotic arm.

The subsequent mechanical investigations of the flexural tensile strength of the geopolymer composites were conducted using 24k carbon fibres impregnated with R1 at an extraction speed of 10 cm/s, due to their higher maximum load and greater E-modulus.

4.3 Mechanical Test

The three-point bending test was conducted on mortar prisms (see Section 4.1), with 4 prisms per series and test point (3, 7, and 28d of curing) tested using a ToniNORM device (Toni Technik GmbH, Berlin, Germany) at a support span of 100 mm and a constant loading rate of 0.05 MPa/s until failure. The investigated sample systems included an unreinforced reference, one freshly impregnated fibre (F_{f1}), one hardened impregnated fibre (F_h , produced exclusively for this laboratory study to highlight the effect of fresh-in-fresh embedding), one non-impregnated fibre (F_u), two freshly impregnated fibres (F_{f2}), and a defective sample with one freshly impregnated fibre displaced after preparation (F_{dis}), with maximum flexural tensile strength calculated from the recorded failure load and prism geometry.

The pullout tests were conducted using a universal testing machine (Z020, ZwickRoell GmbH & Co. KG, Ulm, Germany) with fibre slip determined using an optical displacement sensor (BTC-EXOPTIC.001) by detecting applied displacement markers. After inserting the sample into the machine, the fibre was pulled out vertically, with the mortar-filled mould remaining fixed in position (see Figure 6b-c). After reaching a first preload of 50 N, the test started with a controlled displacement rate of 5 mm/min, applying a single loading ramp. Since only the fibre–mortar bond was being tested, the specimens were not demoulded prior to testing and were measured upside down, with the bottom facing upwards, to ensure a flat top surface and to avoid introducing any moments during the pullout test. To clamp the fibres into the bolt, the upper end was embedded in specially 3D-printed sample holders (see Figure 6a).

Pullout tests were conducted using the F_u and F_{f1} samples with sample ages of 3 and 28d, with 4 specimens per test series.

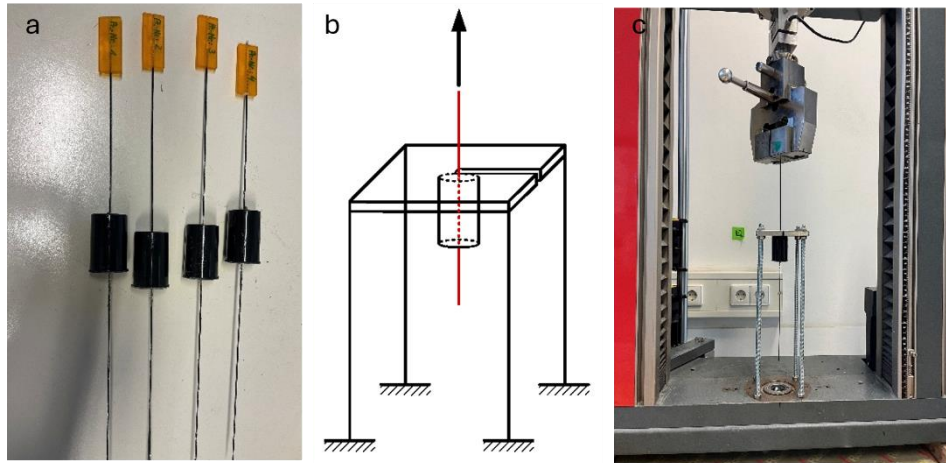


Figure 6. Representation of (a) the test specimen with attached sample holder, (b) schematic diagram of the experimental setup, and (c) the placement of the specimen into the clamping bolt.

The interfacial bond strength τ [MPa] (see Eq. 1) was calculated according to [30,32] based on the maximum recorded pullout force (F_{max}), the fibre diameter (D) and the embedded length of the fibre (l_e), assuming uniform stress distribution along the bond line.

$$\tau = \frac{F_{max}}{\pi \cdot D \cdot l_e} \quad (1)$$

4.4 Microscopic Examinations

SEM images were examined using a Zeiss Gemini SEM500 Nano device equipped with a field-emission cathode and an in-lens detector. Measurements were carried out on thin-section samples taken perpendicular to the fibre direction. The specimens tested at an age of 28d were embedded in EP resin. To ensure proper electron conduction during imaging, the edges of the samples were coated with a conductive silver layer. Imaging was carried out under a vacuum of 100 Pa, with a working distance of 11 mm and an accelerating voltage of 15 kV. Backscattered electron (BSE) images were acquired using a 4-quadrant BSE detector, while secondary electron (SE) images were obtained via the integrated in-lens detector.

Light microscopic examinations were carried out on samples prepared parallel to the fibre direction. The specimens were polished using a Metasinx disc grinder with abrasive paper (grit sizes 60, 120, 240, and 600) under water cooling, and observed with a Zeiss Stemi SV11 stereomicroscope.

5. Results and Discussion

5.1 Mechanical Test Results

The flexural tensile strength was assessed using a three-point bending test (see Section 4.3), revealing clear differences among the various reinforcement strategies. Figure 7 presents the results for the geopolymer's flexural tensile strength when reinforced with continuous carbon fibre strands.

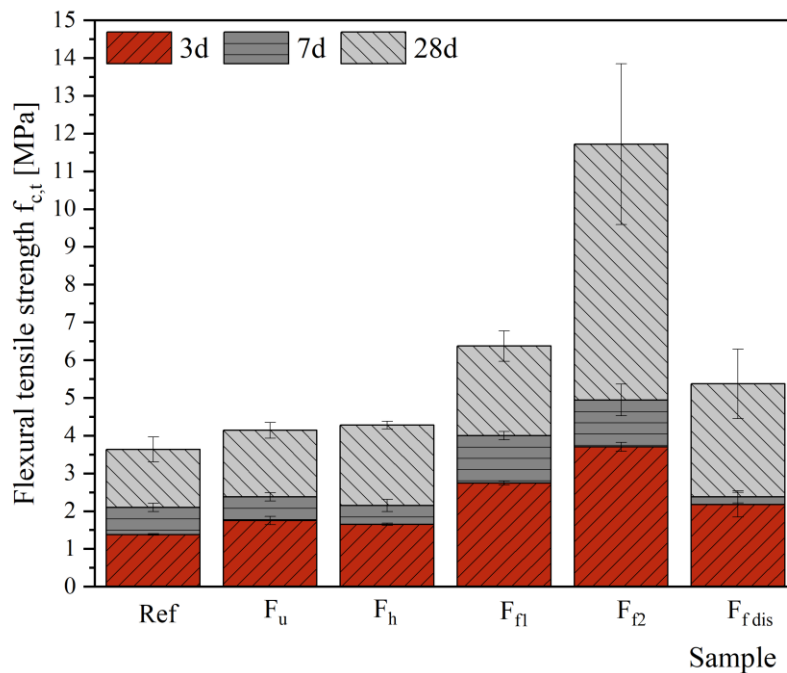


Figure 7. Mean flexural tensile strength at 3, 7, and 28d for the unreinforced 3D-printable geopolymer (Ref); the geopolymer reinforced with a non-impregnated continuous carbon fibre strand (F_u); and with continuous carbon fibre strands impregnated with epoxy resin (F_h , F_{f1} , F_{f2} , and F_{fdis}).

Using non-impregnated fibre strands (F_u), no improvement in flexural strength could be identified when compared to the unreinforced reference samples (Ref). The flexural strength of F_u samples was approx. 1.5 MPa after 3d and approx. 3.5 MPa after 28d, similar to the

reference values. This suggests that the non-impregnated fibres do not provide sufficient resistance within the mortar matrix. Due to a lack of bonding within the geopolymer matrix, the fibres are likely pulled out during loading without contributing significantly to the tensile load transfer.

In a second series, fibre strands with a hardened coating (F_h) were tested. These samples also showed only a slight improvement in flexural strength at any age compared to Ref or F_u , which is somewhat unexpected given that hardened epoxy-impregnated carbon fibres are commonly used in carbon-reinforced concrete. Based on image analysis, the fibres exhibited a clear pull-out failure, indicating a lack of proper bonding between the hardened fibre surface and the matrix. Microscopic investigations and testing suggest that the hardened surface did not develop an adequate fibre-matrix-bond, limiting stress transfer.

A clear increase in flexural strength was observed when freshly impregnated fibre strands (F_{f1}) were applied. At both 3 and 28d, the flexural strength nearly doubled compared to the unreinforced samples (Ref). Notably, after just 7d, the flexural tensile strength of F_{f1} matched the 28d-strength of F_u samples. This suggests that the "fresh-in-fresh" application enables good bonding between the fibre surface and the matrix, resulting in significantly improved load-bearing capacity. Further improvement was achieved by placing two freshly impregnated fibre strands in parallel (F_{f2}) in the tensile zone of the specimen. While only a slight increase compared to F_{f1} was measured at early age (7d), the flexural strength was significantly higher after 28d. On average, values up to 12 MPa were recorded, compared to around 6 MPa for F_{f1} and 3.5 MPa for F_u with the same sample age. This corresponds to a fourfold increase in tensile load capacity compared to the unreinforced reference and a twofold increase compared to the single-strand reinforcement (F_{f1}).

Finally, the importance of accurate fibre placement was investigated using a sample where the freshly impregnated strand was displaced (F_{dis}) after mortar placement and compaction. The results showed a slightly lower flexural strength than F_{f1} and greater variability, especially after 28d. Despite this, an improvement over Ref and F_u was still noticeable. These findings highlight not only the need for careful placement and fixation of the fibres within the print path to ensure reliable and consistent reinforcement performance but also demonstrate the effectiveness of freshly impregnated fibre strands, embedded using a fresh-in-fresh approach, in significantly enhancing tensile load-bearing capacity.

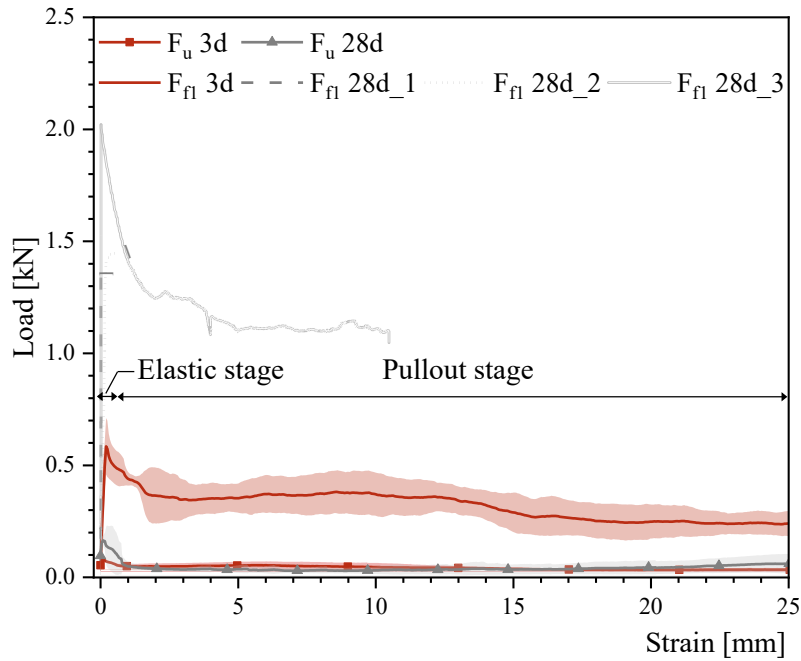


Figure 8. Strain–load diagrams for F_u and F_{f1} specimens after 3 and 28d of curing.

Based on the findings from the flexural tensile strength tests (see Figure 7), pullout tests were carried out only on samples F_u (with non-impregnated fibre strands) and F_{f1} (with one freshly impregnated fibre strand embedded fresh-in-fresh). These two reinforcement systems were selected because they showed the most relevant differences in mechanical behaviour. Furthermore, due to the highest observed strength increases based on flexural tensile strength, only samples aged 3 and 28d were tested. Figure 8 shows the mean strain–load curves from the geopolymer's pullout tests with sample ages of 3 and 28d, including their deviations. An exception was made for sample F_{f1} at 28d, where no mean value could be calculated because some fibres failed before any pullout occurred. This was likely due to the bond strength exceeding the fibre strength. To confirm this hypothesis, a substantially larger number of samples or samples with a shorter embedded length should be investigated. In this study, the individual measurements are shown. Nevertheless, peak load was calculated with fibre failure. The test results at 3d are shown in red, and those at 28d in grey. A significant increase in pullout strength was observed in both series over time.

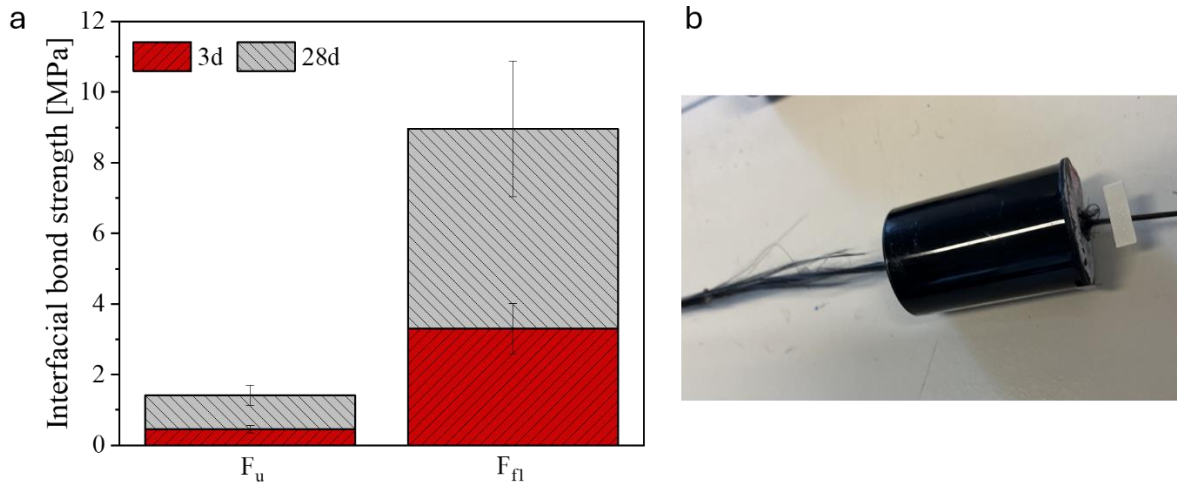


Figure 9. (a) Interfacial bond strength of F_u and F_{f1} after 3 and 28d; (b) F_u sample showing telescopic pullout behaviour.

All samples exhibited a similar characteristic behaviour, showing an initial linear load increase (elastic stage), followed by a peak load at the onset of fibre slippage (pullout stage). It should be noted that the measured strain values include both fibre slippage and the elastic deformation of the fibres. Comparable to [8], only minimal fibre slippage could be observed up to the point of peak load, with measured values ranging from approx. 60 to 160 μm for F_u and 180 to 210 μm for F_{f1} . The load drop after peak load indicates the failure of the fibre-matrix bond. As the fibre is pulled out of the matrix, the load-bearing capacity gradually decreases with increasing pullout length. The effectiveness of the fresh-in-fresh embedding method is clearly visible in the results. While the non-impregnated fibre (F_u) reached an average pullout force of around 100 N at 3d and about 250 N at 28d, F_{f1} showed much higher values: approx. 600 N at 3d and 1700 N at 28d. This corresponds to a fivefold increase in peak load at 3d and nearly a sevenfold increase at 28d.

Remarkably, the 3d result of F_{f1} already exceeded the 28d result of F_u by a factor of 2.5. These findings suggest that the fresh-in-fresh embedding significantly improves the fibre-matrix bond. Concerning the remaining load capacity during the pullout stage, for the F_u samples, it was almost negligible due to the weak fibre-matrix bond. In contrast, Sample F_{f1} continued to transfer load during the pullout stage, as indicated by the strain. At 3d, the remaining load capacity during this stage was, on average, around 50% of the peak load, gradually decreasing to about 30% with increasing strain. For F_{f1} at 28d, this behaviour could not be reliably averaged due to fibre failure. However, one individual measurement still showed a reduced load capacity of approximately 1200 N during the pullout stage, which corresponds to a 40% decrease from the peak load.

Figure 9a shows the calculated interfacial bond strength (IBS), which clearly illustrates the force needed to separate the fibre from the surrounding matrix. The value depends on the peak load in relation to the fibre diameter and the embedded length. The results demonstrate the beneficial effect of fresh-in-fresh embedding, where the freshly impregnated carbon fibre is integrated into the mortar. Compared to the IBS values discussed in Section 2, the IBS measured in this study, with around 9 MPa after 28d for F_{f1} , cannot be directly compared with conventional steel reinforcement with higher bond strengths. However, it clearly demonstrates the effectiveness of the investigated fibre coating technique, especially when compared to the IBS of the non-impregnated fibre F_u , which reached only around 1.5 MPa after 28d, in improving the bond strength for 3D printing applications.

During the pullout test of the F_u samples, it was observed that only the inner filaments were pulled out, while the outer filaments failed due to tensile loading (see Figure 9b). This

indicates that the outer filaments had a stronger bond to the surrounding matrix and could not be pulled out because of higher friction forces. This behaviour is known as 'telescopic pullout' [50,51] and could explain the better bond strength of F_{f1} with pulling out the fibre without separating its filaments as illustrated in Figure 10.

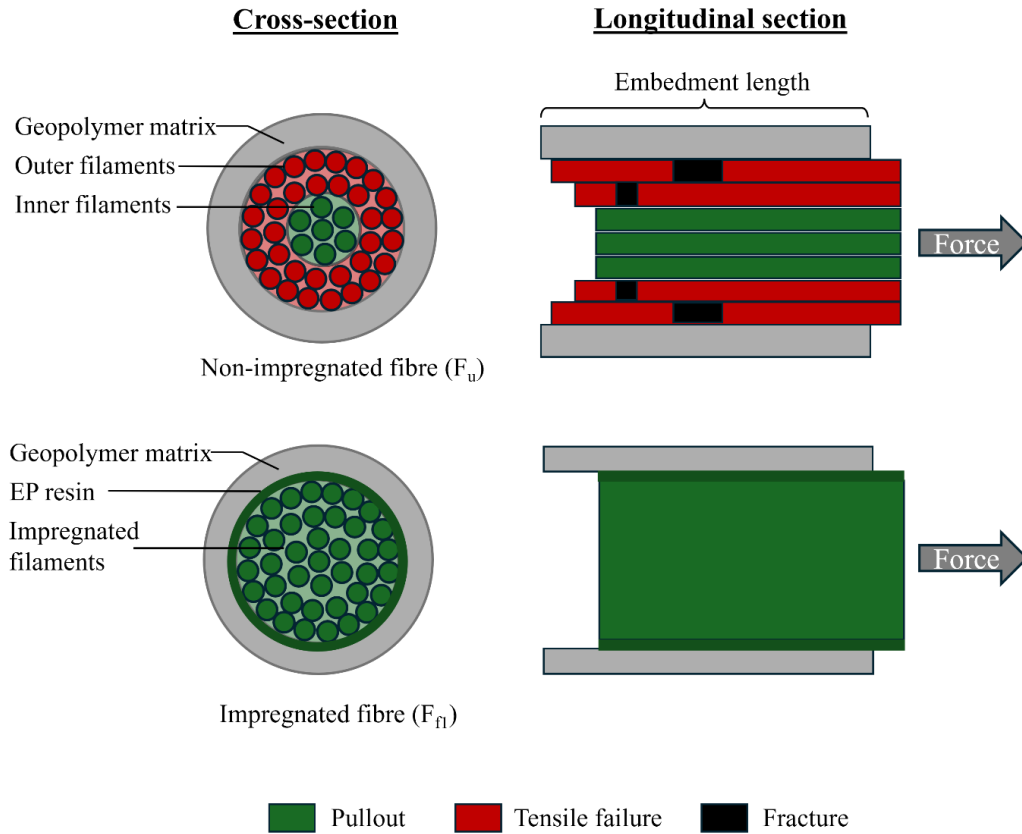


Figure 10. Schematic illustration of fibre pullout for non-impregnated and impregnated fibres, highlighting the telescopic pullout behaviour of non-impregnated fibres according to [51].

In several cases, the fibre–mortar bond proved to be stronger than the fixation of the fibre within the sample holder. As a result, many measurements had to be repeated because the fibre was pulled out from the holder instead of the mortar. This issue must be fixed for future test setups.

5.2 Microscopic Test Results

To assess the mechanical performance and to better understand the fibre–matrix interaction, geopolymer specimens with different fibre embedding techniques were examined using microscopy. These analyses complemented mechanical testing by revealing microstructural features and interfacial characteristics. In the following, SEM images of F_u , F_h and F_f samples (cross-sections perpendicular to the fibres) are discussed. In addition, a light microscopy investigation was conducted on the F_f sample in a longitudinal section parallel to the fibre. Such longitudinal analysis was not possible for the F_u and F_h samples, as the fibres loosened during polishing.

During sample preparation for SEM, which involved embedding in EP resin, images revealed two distinguishable resin types. These could only be differentiated based on brightness contrast: the lighter resin (LR) originated from the original fibre embedding, while the darker resin (DR) was introduced during sample preparation. This is clearly visible in Figure 11b. Small white rod-shaped structures found on all SEM images in the resin areas were identified

via EDX as likely silicon carbide, a known abrasive. These are considered preparation-related errors and are not discussed further.

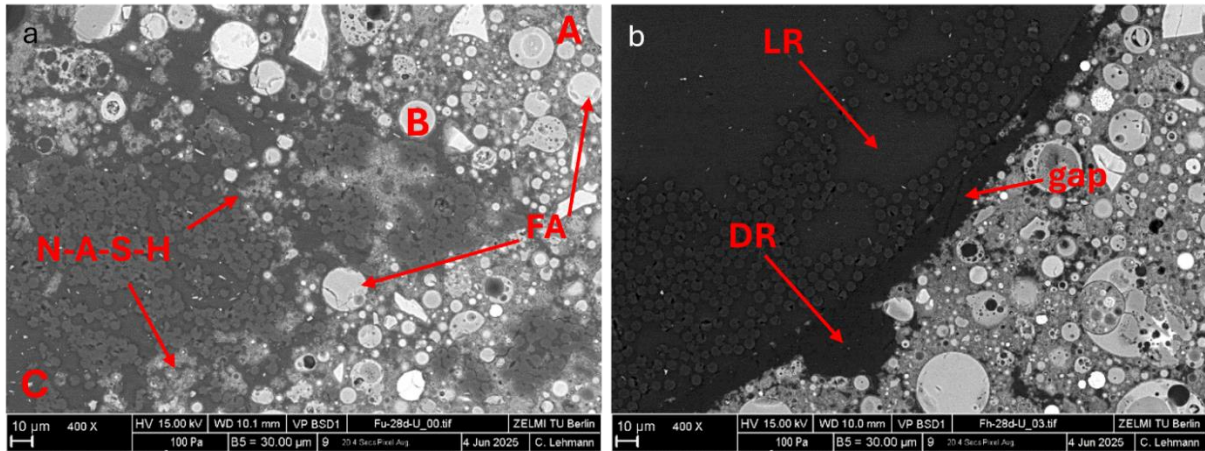


Figure 11. SEM images of fly ash (FA)-based geopolymer with continuous carbon fibre reinforcement: (a) Sample F_u (non-impregnated fibre), revealing three distinct regions: (A) geopolymer matrix, (B) transition zone, and (C) the fibre bundle; and (b) Sample F_h (impregnated fibre) revealing only the geopolymer matrix and the fibre bundle with the lighter resin (LR) originated from the original fibre embedding and darker resin (DR) from sample preparation.

The SEM analysis of F_u samples (Figure 11a) revealed three distinct regions: (A) geopolymer matrix, (B) transition zone, and (C) the fibre bundle with individual filaments. Within the transition area, N-A-S-H-like reaction products were observed to grow into the fibre, forming a 'fluffy' texture typical of amorphous phases. The presence of resin within the fibre bundle and surrounding transition zone indicates insufficient bonding between fibre and matrix. This likely allowed the fibre to loosen during sample grinding, which could explain the low flexural tensile strength and low pullout resistance observed for these samples. The telescopic pullout behaviour may result from increased friction at the transition area, where reaction products penetrate the fibre, possibly leading to fibre fracture (see Figure 10).

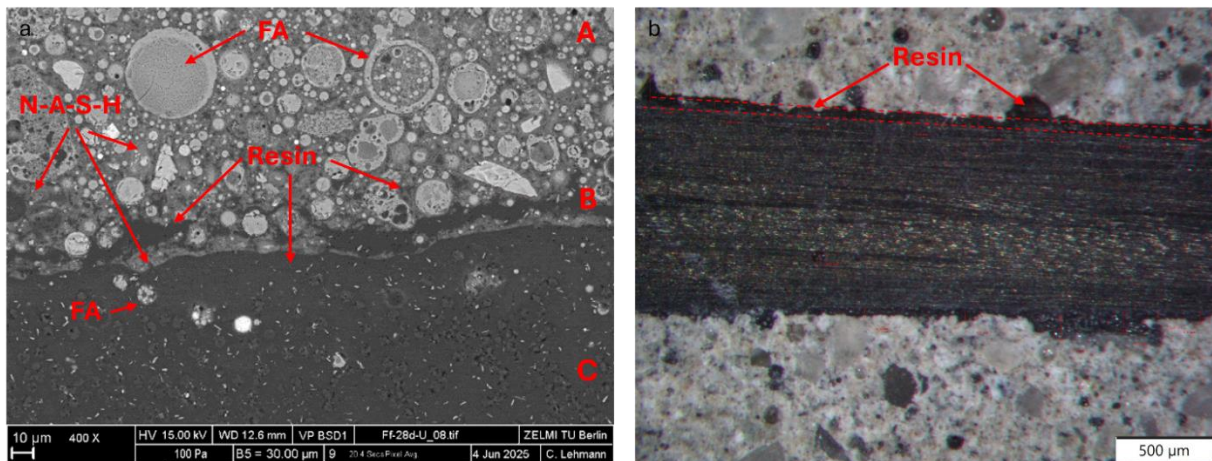


Figure 12. Microscopy results of fly ash (FA)-based geopolymer with "fresh-in-fresh" embedded carbon fibre: (a) SEM cross-section, revealing three distinct regions: (A) geopolymer matrix, (B) transition zone, and (C) the fibre bundle; and (b) light microscopy of longitudinal section with epoxy surface.

F_h samples, which also showed low flexural strength, presented in SEM images a clear separation between the fibre bundle and surrounding matrix (Figure 11b). These fibres were pre-impregnated with resin and inserted into hardened mortar. The analysis revealed internal air voids within the bundle and a thin resin layer around the fibres. While initial contact between

fibre and matrix may have existed (A), it was disrupted during sample preparation. The resulting gap was filled with darker EP resin. This weak bonding supports the low flexural tensile strength observed for these samples.

In contrast, the "fresh-in-fresh" embedded F_f samples revealed improved fibre–matrix interaction. SEM images revealed geopolymer mortar with N-A-S-H phases as reaction product with the inserted fibre bundle with internal filaments surrounded by a thick resin coating (Figure 12a). As in the F_u samples, distinct mortar (A), transition (B), and fibre (C) zones were visible. However, in F_f samples, the original resin appeared to have penetrated the fresh mortar, forming mechanical interlocks through infiltration of capillary pores and surface roughness within the uncured matrix, indicating stronger mechanical bonding. This effect has also been reported in previous studies by other researchers [29]. As discussed in Section 3, resin penetration enhances adhesion through van der Waals forces and micro-mechanical anchoring, especially in the presence of fine matrix irregularities. Some fly ash spheres penetrated the fibre bundle and underwent geopolymerisation, although there was insufficient space for the full development of reaction products. This corresponds with the higher pullout forces measured in mechanical tests. Light microscopy of the F_f sample further supported these findings. As shown in Figure 12b, the mortar matrix enclosed the embedded fibre, which was impregnated on both sides with an irregular resin layer approx. 0.05 mm thick, as marked in Figure 12b. The uneven surface contour suggests numerous anchoring points between the impregnated fibre and the geopolymer. The presence of uncured EP in the fresh matrix allows intimate contact and setting in place, promoting both adhesive and cohesive interfacial strength as the system hardens. In addition, individual resin droplets (approx. 0.15 mm thickness) were observed at the fibre edge, which may contribute further to mechanical anchorage and resistance against pullout. These droplets can act as mechanical locks, increasing the energy required for fibre extraction. This confirms the assumption of a complete fibre pullout mechanism due to the strong bond strength and high pullout resistance shown in Figure 10.

6. Conclusion and Future Perspectives

This study examined different strategies for embedding continuous carbon fibres into 3D-printable fly ash-based geopolymers. Among all tested methods, the "fresh-in-fresh" approach showed the best performance. Non-impregnated (F_u) and pre-impregnated fibres embedded hardened into the mortar (F_h) did not significantly improve flexural strength compared to unreinforced samples, reaching only about 3.5 MPa after 28d. Microscopy analysis confirmed weak fibre-matrix bonding, explaining the low load transfer and poor mechanical performance.

In contrast, F_f samples, where freshly impregnated fibres were embedded into fresh mortar, achieved up to 6 MPa (F_{f1}) and even 12 MPa with two strands (F_{f2}), indicating strong load-bearing capability. Microscopic observations revealed effective resin integration and anchorage within the matrix, driven by the infiltration of uncured resin into the fresh mortar. This promotes mechanical interlock and chemical adhesion during curing, significantly enhancing the interfacial bond strength.

Pullout tests further confirmed this, with F_{f1} samples showing peak loads up to seven times higher than F_u . The high interfacial bond strength (approx. 9 MPa at 28d) highlights the potential of the "fresh-in-fresh" embedding for reinforcing 3D-printed geopolymers.

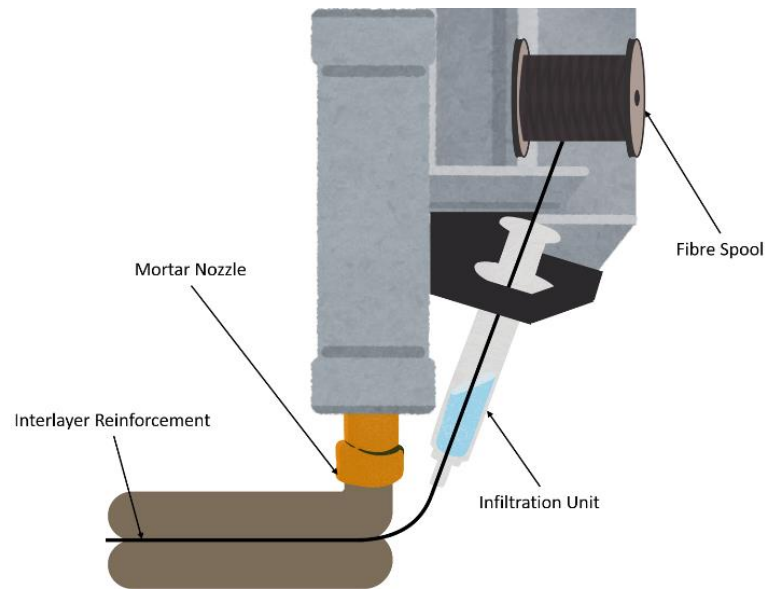


Figure 13. Integration impregnation system on extruder printhead; the fibre, anchored to the mortar bottom layer, is pulled along the top layer by the force exerted through material extrusion.

As 3D printing aims for a fully automated construction method, in situ fibre infiltration is essential. It not only enables automation but also demonstrates the best mechanical performance in this study. The newly developed print head, featuring a fibre impregnation unit, cutting device, and fibre laying mechanism, is schematically shown in Figure 13. Three different nozzles with 0°, 45° and 90° angles can be used to minimise the fibre extraction force. This setup allows the use of EP-impregnated carbon fibre strands embedded fresh-in-fresh into the mortar. This technique is suitable for 3D geopolymers and concrete printing applications.

Data availability statement

Data will be made available on request.

Underlying and related material

-

Author contributions

Mona Sando: Conceptualization, Data curation, Formal Analysis, Investigation, Methodology, Project administration, Resources, Validation, Visualization, Writing – original draft, Writing – review & editing; **Sara Alves Santos:** Data curation, Formal Analysis, Investigation, Methodology, Resources, Validation, Visualization, Writing – original draft; **Paul Worms:** Investigation, Methodology, Validation, Visualization; **Aleksander Gurlo:** Funding acquisition, Project administration, Supervision; **Dietmar Stephan:** Funding acquisition, Project administration, Supervision, Writing – review & editing

Competing interests

The authors declare that they have no competing interests.

Funding

The project on which this paper is based is by the State of Berlin, Germany, within the context of the Programme for the Support of Research, Innovation and Technologies (Pro FIT) under application number 10189161.

Acknowledgement

The authors would like to thank Lisa-Marie Kaufmann, Chaitanya Singh and Dr Ulla Simon for their support in the laboratory and their contribution to the development of practical implementation ideas. We also thank Dr Christian Lehmann for his support with SEM.

References

- [1] S. Lim, R. Buswell, T. Le, R. Wackrow, S. Austin, A. Gibb, T. Thorpe, Development of a Viable Concrete Printing Process, in: 28th International Symposium on Automation and Robotics in Construction (ISARC 2011), n.d. <https://doi.org/10.22260/ISARC2011/0124>.
- [2] M. Sando, D. Stephan, The role of mixing sequence in shaping the 3D-printability of geopolymers, *Case Studies in Construction Materials* 22 (2025) e04352. <https://doi.org/10.1016/j.cscm.2025.e04352>.
- [3] M. Sando, D. Stephan, Online monitoring for 3D printable geopolymers: Automated slug test analysis with image analysis revealing mixing sequence effects, *Construction and Building Materials* 490 (2025) 142480. <https://doi.org/10.1016/j.conbuildmat.2025.142480>.
- [4] H. Kloft, M. Empelmann, N. Hack, E. Herrmann, D. Lowke, Reinforcement strategies for 3D-concrete-printing, *Civil Engineering Design* 2 (2020) 131–139. <https://doi.org/10.1002/cend.202000022>.
- [5] O. Zaid, M.H. El Ouni, Advancements in 3D printing of cementitious materials: A review of mineral additives, properties, and systematic developments, *Construction and Building Materials* 427 (2024) 136254. <https://doi.org/10.1016/j.conbuildmat.2024.136254>.
- [6] Carbocon, The carbon concrete principal, (n.d.). <https://www.carbocon.de/en/carbon-concrete/> (accessed September 9, 2025).
- [7] F.C. Campbell, ed., *Structural composite materials*, ASM International, Materials Park, Ohio, 2010.
- [8] T. Neef, S. Müller, V. Mechtcherine, Integrating continuous mineral-impregnated carbon fibers into digital fabrication with concrete, *Materials & Design* 239 (2024) 112794. <https://doi.org/10.1016/j.matdes.2024.112794>.
- [9] Y. Liu, B. Zwingmann, M. Schlaich, Carbon Fiber Reinforced Polymer for Cable Structures—A Review, *Polymers* 7 (2015) 2078–2099. <https://doi.org/10.3390/polym7101501>.
- [10] A. Carolin, Carbon fibre reinforced polymers for strengthening of structural elements, Luleå University of Technology, Department of Civil, Environmental and Natural Resources Engineering, 2003. <https://urn.kb.se/resolve?urn=urn:nbn:se:ltu:diva-16879>.
- [11] J.G. Teng, T. Yu, D. Fernando, Strengthening of steel structures with fiber-reinforced polymer composites, *Journal of Constructional Steel Research* 78 (2012) 131–143. <https://doi.org/10.1016/j.jcsr.2012.06.011>.
- [12] D.S. Vijayan, A. Sivasuriyan, P. Devarajan, A. Stefańska, Ł. Wodzyński, E. Koda, Carbon Fibre-Reinforced Polymer (CFRP) Composites in Civil Engineering Application—A Comprehensive Review, *Buildings* 13 (2023) 1509. <https://doi.org/10.3390/buildings13061509>.
- [13] E. Ivaniuk, S. Müller, T. Neef, V. Mechtcherine, Strategies for Integrating Reinforcement Into 3D Concrete Printing at the TU Dresden, *Open Conf Proc* 1 (2022) 23–34. <https://doi.org/10.52825/ocp.v1i.73>.
- [14] T. Marchment, J. Sanjayan, Mesh reinforcing method for 3D Concrete Printing, *Automation in Construction* 109 (2020) 102992. <https://doi.org/10.1016/j.autcon.2019.102992>.
- [15] L. Gebhard, J. Mata-Falcón, A. Iqbal, W. Kaufmann, Structural behaviour of post-installed reinforcement for 3D concrete printed shells – A case study on water tanks, *Construction*

- p and Building Materials 366 (2023) 130163.
- <https://doi.org/10.1016/j.conbuildmat.2022.130163>
- .
- [16] L. Gebhard, P. Bischof, A. Anton, J. Mata-Falc3n, B. Dillenburger, W. Kaufmann, Pre-installed Reinforcement for 3D Concrete Printing, in: A.B. Richard Buswell Sergio Cavalaro, Peter Kinnell (Ed.), Digital Concrete 2022, Springer Cham, n.d.: pp. 430–435. https://doi.org/10.1007/978-3-031-06116-5_64.
- [17] Z. Xia, J. Geng, Z. Zhou, G. Liu, Comparative analysis of polypropylene, basalt, and steel fibers in 3D printed concrete: Effects on flowability, printability, rheology, and mechanical performance, Construction and Building Materials 465 (2025) 140098. <https://doi.org/10.1016/j.conbuildmat.2025.140098>.
- [18] F.P. Bos, Z.Y. Ahmed, R.J.M. Wolfs, T.A.M. Salet, 3D Printing Concrete with Reinforcement, in: D. Hordijk Luković, M. (Ed.), High Tech Concrete: Where Technology and Engineering Meet, Springer Cham, 2018: pp. 2484–2493. https://doi.org/10.1007/978-3-319-59471-2_283.
- [19] J.-F. Caron, N. Ducoulombier, L. Demont, V. Bono, R. Mesnil, 3D Printing of Continuous-Fibers Cementitious Composites, Open Conf Proc 3 (2023). <https://doi.org/10.52825/ocp.v3i.193>.
- [20] J.H. Lim, B. Panda, Q.-C. Pham, Improving flexural characteristics of 3D printed geopolymer composites with in-process steel cable reinforcement, Construction and Building Materials 178 (2018) 32–41. <https://doi.org/10.1016/j.conbuildmat.2018.05.010>.
- [21] L. Demont, N. Ducoulombier, R. Mesnil, J.-F. Caron, Flow-based pultrusion of continuous fibers for cement-based composite material and additive manufacturing: rheological and technological requirements, Composite Structures 262 (2021) 113564. <https://doi.org/10.1016/j.compstruct.2021.113564>.
- [22] W. Dong, J. Zhao, B. Yang, M. Liebscher, V. Mechtcherine, Early strength enhancement of cementitious mineral-impregnated carbon fibre (MCF) reinforcements via electric Joule heating, Construction and Building Materials 489 (2025) 142231. <https://doi.org/10.1016/j.conbuildmat.2025.142231>.
- [23] C. Signorini, A.H. Ahmed, M. Liebscher, J. Zhao, T. Köberle, V. Mechtcherine, Hybrid fibre-reinforced cementitious composites with short polyethylene and continue carbon fibres: Influence of roving impregnation on tensile and cracking behaviour, Materials & Design 248 (2024) 113465. <https://doi.org/10.1016/j.matdes.2024.113465>.
- [24] J. Zhao, P. van Tai, A.B. Rezaie, B. Fan, M. Liebscher, V. Mechtcherine, Enhanced impregnation quality, interfacial bonding, and mechanical performance of cementitious mineral-impregnated carbon fiber reinforcements through tailored fiber sizing, Composites Part B: Engineering 305 (2025) 112707. <https://doi.org/10.1016/j.compositesb.2025.112707>.
- [25] J. Bielak, J. Schöneberg, M. Classen, J. Hegger, Shear capacity of continuous concrete slabs with CFRP reinforcement, Construction and Building Materials 320 (2022) 126117. <https://doi.org/10.1016/j.conbuildmat.2021.126117>.
- [26] M. Glowania, T. Gries, J. Schoene, M. Schleser, U. Reisgen, Innovative Coating Technology for Textile Reinforcements of Concrete Applications, KEM 466 (2011) 167–173. <https://doi.org/10.4028/www.scientific.net/KEM.466.167>.
- [27] M. Scheurer, G. Dittel, M. Kalthoff, M. Raupach, T. Matschei, T. Gries, Evaluation of Properties of Impregnated Reinforcement Textiles Cured Within Concrete for Applications in Concrete Extrusion, in: A. Ilki, D. Çavunt, Y.S. Çavunt (Eds.), Building for the Future: Durable, Sustainable, Resilient, Springer Nature Switzerland, Cham, 2023: pp. 1293–1302. https://doi.org/10.1007/978-3-031-32519-9_131.
- [28] M. Scheurer, M. Kalthoff, T. Matschei, M. Raupach, T. Gries, Analysis of Curing and Mechanical Performance of Pre-Impregnated Carbon Fibers Cured within Concrete, Textiles 2 (2022) 657–672. <https://doi.org/10.3390/textiles2040038>.
- [29] M. Scheurer, D. Friese, P. Penzel, G. Dittel, S. Bhat, V. Overhage, L. Hahn, K. Heins, C. Cherif, T. Gries, Current and Future Trends in Textiles for Concrete Construction Applications, Textiles 3 (2023) 408–437. <https://doi.org/10.3390/textiles3040025>.

- [30] V. Bilek, S. Bonczková, J. Hurta, D. Pytlík, M. Mrovec, Bond Strength Between Reinforcing Steel and Different Types of Concrete, *Procedia Engineering* 190 (2017) 243–247. <https://doi.org/10.1016/j.proeng.2017.05.333>.
- [31] Eurocode 2 – Background and applications – Design of concrete buildings. Worked examples, Publications Office of the European Union, n.d. <https://doi.org/10.2788/35386>.
- [32] Q. Yuan, J. Yang, K. Zhang, X. Long, Q. Li, J. Zou, Interfacial bonding properties of novel strand steel fiber and cement matrix: Experimental and analytical investigations, *Construction and Building Materials* 472 (2025) 140835. <https://doi.org/10.1016/j.conbuildmat.2025.140835>.
- [33] M.G. Alberti, A. Enfedaque, J.C. Gálvez, A. Ferreras, Pull-out behaviour and interface critical parameters of polyolefin fibres embedded in mortar and self-compacting concrete matrixes, *Construction and Building Materials* 112 (2016) 607–622. <https://doi.org/10.1016/j.conbuildmat.2016.02.128>.
- [34] R. Devaraj, A. Olofinjana, C. Gerber, On the Factors That Determine the Bond Behaviour of GFRP Bars to Concrete: An Experimental Investigation, *Buildings* 13 (2023). <https://doi.org/10.3390/buildings13112896>.
- [35] L. Gebhard, L. Esposito, C. Menna, J. Mata-Falcón, Inter-laboratory study on the influence of 3D concrete printing set-ups on the bond behaviour of various reinforcements, *Cement and Concrete Composites* 133 (2022) 104660. <https://doi.org/10.1016/j.cemcon-comp.2022.104660>.
- [36] J. Duan, S. Sun, S. Chi, C. Hu, C. Ling, H. Fu, Z. Han, Effect of process parameters on forming quality and flexural strength of continuous fiber reinforced cement-based 3D printed composites, *Construction and Building Materials* 438 (2024) 137241. <https://doi.org/10.1016/j.conbuildmat.2024.137241>.
- [37] S.A. Mirdehghan, Fibrous polymeric composites, (n.d.) 1–58. <https://doi.org/10.1016/B978-0-12-824381-7.00012-3>.
- [38] Y. Liu, B. Zwingmann, M. Schlaich, Carbon Fiber Reinforced Polymer for Cable Structures—A Review, *Polymers* 7 (2015) 2078–2099. <https://doi.org/10.3390/polym7101501>.
- [39] Y. Li, J. Zhang, Y. He, G. Huang, J. Li, Z. Niu, B. Gao, A review on durability of basalt fiber reinforced concrete, *Composites Science and Technology* 225 (2022) 109519. <https://doi.org/10.1016/j.compscitech.2022.109519>.
- [40] Q. Zu, M. Solvang, H. Li, Commercial Glass Fibers, (n.d.) 1–87. https://doi.org/10.1007/978-3-030-72200-5_1.
- [41] T.K. Das, P. Ghosh, N.Ch. Das, Preparation, development, outcomes, and application versatility of carbon fiber-based polymer composites: a review, *Adv Compos Hybrid Mater* 2 (2019) 214–233. <https://doi.org/10.1007/s42114-018-0072-z>.
- [42] P. Lauff, P. Pugacheva, M. Rutzen, U. Weiß, O. Fischer, D. Volkmer, M.A. Peter, C.U. Grosse, Evaluation of the Behavior of Carbon Short Fiber Reinforced Concrete (CSFRC) Based on a Multi-Sensory Experimental Investigation and a Numerical Multiscale Approach, *Materials (Basel, Switzerland)* 14 (2021). <https://doi.org/10.3390/ma14227005>.
- [43] R. Khan, Fiber bridging in composite laminates: A literature review, *Composite Structures* 229 (2019) 111418. <https://doi.org/10.1016/j.compstruct.2019.111418>.
- [44] P. Penzel, M. May, L. Hahn, S. Scheerer, H. Michler, M. Butler, M. Waldmann, M. Curbach, C. Cherif, V. Mechtcherine, Bond Modification of Carbon Rovings through Profiling, *Materials (Basel, Switzerland)* 15 (2022). <https://doi.org/10.3390/ma15165581>.
- [45] J.D. Ortiz, S.S. Khedmatgozar Dolati, P. Malla, A. Nanni, A. Mehrabi, FRP-Reinforced/Strengthened Concrete: State-of-the-Art Review on Durability and Mechanical Effects, *Materials (Basel, Switzerland)* 16 (2023). <https://doi.org/10.3390/ma16051990>.
- [46] J.-P. Pascault, R.J.J. Williams, Overview of thermosets: structure, properties and processing for advanced applications, (n.d.) 3–27. <https://doi.org/10.1533/9780857097637.1.3>.
- [47] A. Szweczek, G. Łagód, Adhesion of Modified Epoxy Resin to a Concrete Surface, *Materials (Basel, Switzerland)* 15 (2022). <https://doi.org/10.3390/ma15248961>.
- [48] EN 196-1:2016-11, Methods of testing cement - Part 1: Determination of strength; German version EN 196-1:2016, DIN Media GmbH, Berlin, n.d. <https://doi.org/10.31030/2482416>.

- [49] M. Sando, D. Stephan, The development of a fly ash-based geopolymer for extrusion-based 3D printing, along with a printability prediction method, *Case Studies in Construction Materials* 21 (2024) 03407. <https://doi.org/10.1016/j.cscm.2024.e03407>.
- [50] A. Badanoiu, J. Holmgren, Cementitious composites reinforced with continuous carbon fibres for strengthening of concrete structures, *Cement and Concrete Composites* 25 (2003) 387–394. [https://doi.org/10.1016/S0958-9465\(02\)00054-9](https://doi.org/10.1016/S0958-9465(02)00054-9).
- [51] B. Banholzer, Bond of a strand in a cementitious matrix, *Mater Struct* 39 (2006) 1015–1028. <https://doi.org/10.1617/s11527-006-9115-y>.